Applied Physics Express

The Japan Society of Applied Physics

ACCEPTED MANUSCRIPT • OPEN ACCESS

Triarylborane-based thermally activated delayed fluorescence materials with an efficient reverse intersystem crossing

To cite this article before publication: Ryosuke Okumura *et al* 2024 *Appl. Phys. Express* in press https://doi.org/10.35848/1882-0786/ad392a

Manuscript version: Accepted Manuscript

Accepted Manuscript is "the version of the article accepted for publication including all changes made as a result of the peer review process, and which may also include the addition to the article by IOP Publishing of a header, an article ID, a cover sheet and/or an 'Accepted Manuscript' watermark, but excluding any other editing, typesetting or other changes made by IOP Publishing and/or its licensors"

This Accepted Manuscript is **© 2024 The Author(s). Published on behalf of The Japan Society of Applied Physics by IOP Publishing Ltd**.

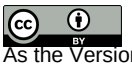

As the Version of Record of this article is going to be / has been published on a gold open access basis under a CC BY 4.0 licence, this Accepted Manuscript is available for reuse under a CC BY 4.0 licence immediately.

Everyone is permitted to use all or part of the original content in this article, provided that they adhere to all the terms of the licence https://creativecommons.org/licences/by/4.0

Although reasonable endeavours have been taken to obtain all necessary permissions from third parties to include their copyrighted content within this article, their full citation and copyright line may not be present in this Accepted Manuscript version. Before using any content from this article, please refer to the Version of Record on IOPscience once published for full citation and copyright details, as permissions may be required. All third party content is fully copyright protected and is not published on a gold open access basis under a CC BY licence, unless that is specifically stated in the figure caption in the Version of Record.

View the article online for updates and enhancements.

This content was downloaded from IP address 18.119.107.161 on 29/04/2024 at 22:57

Template for APEX (Mar. 2022)

Triarylborane-based thermally activated delayed fluorescence materials with an efficient reverse intersystem crossing

Ryosuke Okumura,[1] Yu Kusakabe,[1] Florian Rauch,[2] Lukas Lubczyk,[2] Katsuaki Suzuki,[1] Todd B. Marder,[2]* and Hironori Kaji[1]*

[1] *Institute for Chemical Research, Kyoto University, Uji, Kyoto, 661-0011, Japan*

E-mail: kaji@scl.kyoto-u.ac.jp

[2] *Institut für Anorganische Chemie and Institute for Sustainable Chemistry & Catalysis with Boron, Julius-Maximilians-Universität Würzburg, Am Hubland, 97074 Würzburg, Germany*

E-mail: todd.marder@uni-wuerzburg.de

Efficient reverse intersystem crossing (RISC) is an important process for thermally activated delayed fluorescence (TADF) to suppress efficiency roll-off in organic light-emitting diodes (OLEDs). Enhancing spin-orbit coupling is effective for fast RISC, which is achieved by mediating a locally excited triplet state when RISC occurs between charge transfer states. Here, we experimentally confirmed that efficient RISC occurred in triarylborane-based TADF emitters named **Phox-$^{Me}\pi$**, **Phox-$^{MeO}\pi$**, and **^{MeO3}Ph-$^{FMe}\pi$**. The three emitters showed large rate constants of RISC exceeding 10^6 s^{-1}. **Phox-$^{Me}\pi$**-based OLED exhibited higher maximum external quantum efficiency (EQE_{max} = 10.0%) compared to **Phox-$^{MeO}\pi$**-based OLED (EQE_{max} = 6.7%).

Accepted Manuscript

Organic light-emitting diodes (OLEDs) have attracted considerable attention for their application in displays due to their thinness, light weight, and flexibility.[1–4] The recombination of holes and electrons generates 25% of singlet and 75% of triplet excitons in the emitting layer of OLEDs,[5,6] of which only 25% are available as light in conventional fluorescent materials. Therefore, the theoretical limit of internal quantum efficiency (IQE) had been 25%.[7,8] Although phosphorescent materials can utilize all excitons (IQE = 100%) using iridium or platinum, this leads to high production costs.[9–15] Recently, Adachi et al. successfully demonstrated highly efficient OLEDs using thermally activated delayed fluorescence (TADF) materials as emitters.[16–18] TADF molecules can harvest triplet excitons as well as singlet excitons as light via reverse intersystem crossing (RISC) and subsequent radiative decay, realizing IQE of 100% without the use of metallic elements. The RISC needs to be fast to avoid the accumulation of triplet excitons in OLEDs especially at high current density; otherwise, undesirable efficiency roll-offs occur due to triplet-related annihilations.[19–21] The rate constant of RISC (k_{RISC}) is described by Eq. (1).[22]

$$k_{\mathrm{RISC}} \propto \left|\langle \mathrm{S}|\widehat{H}_{\mathrm{SOC}}|\mathrm{T}\rangle\right|^2 \exp\left(-\frac{\Delta E_{\mathrm{ST}}}{k_{\mathrm{B}}T}\right) \quad (1)$$

Here, $\langle \mathrm{S}|\widehat{H}_{\mathrm{SOC}}|\mathrm{T}\rangle$, k_{B}, T, and ΔE_{ST} represent the spin-orbit coupling (SOC) matrix element value between singlet (S) and triplet (T) states, Boltzmann constant, temperature, and energy gap between the lowest excited singlet (S_1) and lowest triplet (T_1) states, respectively. Equation (1) indicates that minimizing ΔE_{ST} and enhancing SOC play important roles in accelerating RISC. Conventionally, the strategy of separating the highest occupied molecular orbital (HOMO) and lowest unoccupied molecular orbital (LUMO) has been adopted to achieve small ΔE_{ST} for TADF molecules composed of electron donor (D) and acceptor (A) segments. However, in this case, both S_1 and T_1 tend to have charge transfer (CT) type character (denoted as ^{1}CT and ^{3}CT, respectively),[23,24] resulting in negligibly small SOC between them as per El-Sayed's rule.[25] One effective solution to enhance SOC without employing the heavy atom effect is to mediate a locally excited triplet state (^{3}LE) in RISC between ^{1}CT and ^{3}CT.[23,26,27]

Based on our quantum chemical calculations, and our extensive experience in developing 3-coordinate boron compounds for a wide range of applications,[28-34] we recently designed,

Accepted Manuscript

synthesized, and characterized three triarylborane-based TADF emitters, namely **Phox-^{Me}π**, **Phox-^{MeO}π**, and **^{MeO3}Ph-^{Fme}π**, (Fig. 1).[35] **Phox-^{MeO}π** and **^{MeO3}Ph-^{FMe}π** were designed to enhance SOC by minimizing ^{1}CT (S_1)-^{3}LE (T_2) energy gap. As illustrated in Fig. 1, the second (T_2) and third (T_3) lowest triplet states of **Phox-^{Me}π** are both LE type (^3LE_D: LE confined on donor and $^3LE_\pi$: LE confined on the π-bridge, respectively), but are 0.23 eV and 0.58 eV higher than the T_1 state, respectively, indicating that they cannot participate in the RISC process. To lower the energy level of the ^{3}LE state, different substitutions were introduced at the π-bridge, rather than at the donor or acceptor moiety, because we can change the energy level of the LE state without changing those of the CT states. In **Phox-^{MeO}π**, two electron donating (OMe) groups were introduced into the π-bridge to achieve a small T_1 (^{3}CT)-T_2 ($^3LE_\pi$) energy gap. **^{MeO3}Ph-^{FMe}π** was designed to raise the energy levels of the S_1 (^{1}CT) and T_1 (^{3}CT) states by replacing the donor segment with a weaker 2,4,6-trimethoxyphenyl donor, and to reduce the T_1 (^{3}CT)-T_2 ($^3LE_\pi$) energy gap by introducing electron withdrawing (CF_3) groups at the π-bridge. These strategies were expected to provide fast RISC via the $^3LE_\pi$ (T_2) state for both **Phox-^{MeO}π** and **^{MeO3}Ph-^{Fme}π**.

Herein, we investigated the photophysical properties of doped films of these emitters to confirm the design concept mentioned above and then fabricated OLEDs using these emitters. The photophysical measurements revealed that **Phox-^{Me}π**, **Phox-^{MeO}π**, and **^{MeO3}Ph-^{FMe}π** exhibited short delayed fluorescence lifetimes (τ_{DF}) of 1.4, 0.9, and 3.2 μs, respectively. **Phox-^{MeO}π** and **^{MeO3}Ph-^{FMe}π** showed large k_{RISC}s of 1.6×10^6 and 2.0×10^6 s^{-1} as expected. Contrary to our expectation, **Phox-^{Me}π** also showed a large k_{RISC} of 2.6×10^6 s^{-1}. **Phox-^{Me}π** and **Phox-^{MeO}π**-based OLEDs provided maximum external quantum efficiencies (EQE_{max}) of 10.0% and 6.7%, respectively (their photoluminescence quantum yields (PLQYs, Φ_{PLS}) were 70 and 36%, respectively, *vide infra*).

Photophysical properties were measured for **Phox-^{Me}π**, **Phox-^{MeO}π**, and **^{MeO3}Ph-^{FMe}π** doped films. The emission colors of **Phox-^{Me}π**, **Phox-^{MeO}π**, and **^{MeO3}Ph-^{FMe}π** ranged from sky-blue to reddish. Therefore, we selected the most representative and widely used 3,3′-di(9H-carbazol-9-yl)-1,1′-biphenyl (mCBP) as the host, which can cover the wide range of emissions. Figure 2(a) shows their photoluminescence (PL) spectra with photoluminescence peak wavelengths (λ_{PL}) of 581, 626, and 484 nm for **Phox-^{Me}π**, **Phox-^{MeO}π**, and **^{MeO3}Ph-^{FMe}π**, respectively. The broad emissions confirmed the results of quantum chemical

Accepted Manuscript

calculations that their S_1 states have CT character. The PLQYs of 70%, 36%, and 50% were obtained for **Phox-$^{Me}\pi$**, **Phox-$^{MeO}\pi$**, and **^{MeO3}Ph-$^{FMe}\pi$**, respectively (Table 1). As **^{MeO3}Ph-$^{FMe}\pi$** exhibited blue emission, we further investigated the behavior of λ_{PL} and Φ_{PL} at different doping concentrations (10, 20%, and 100% (neat) films). As exhibited in Table SIII, Commission Internationale de l'Ecairage (CIE) y values increased with increasing doping concentrations from 5 to 20%, but decreased for the neat film. This behavior was the same as that previously reported for blue TADF emitters.[36,37] Moreover, Φ_{PL}s increased with increasing doping concentrations, reaching 79% in the neat film.

We have further investigated the photophysical behavior of **^{MeO3}Ph-$^{FMe}\pi$** in a different host, namely 2,8-bis(diphenylphosphoryl)dibenzo[b,d]furan (PPF), because it has a higher T_1 energy (3.1 eV[38]), which is suitable for blue TADF emitters. The Φ_{PL} of **^{MeO3}Ph-$^{FMe}\pi$** in PPF was 79% at 20 wt%, which was higher than that in mCBP (54%). The emission wavelength was slightly red-shifted (λ_{PL} = 490 nm) (Table SIV).

Figure 2(b) displays the experimental transient PL decay curves; the lifetimes of prompt fluorescence (τ_{PF}) were 60.0, 31.9, and 82.5 ns and τ_{DF} were 1.4, 0.9, and 3.2 μs for **Phox-$^{Me}\pi$**, **Phox-$^{MeO}\pi$**, and **^{MeO3}Ph-$^{FMe}\pi$**, respectively. All emitters showed relatively short τ_{DF}s (~ 1–3 μs), originating from fast RISC and the subsequent radiative decay. Table I shows the photophysical properties including the rate constants (see Eqs. S1–S4 for the derivation).[27] The k_{RISC}s of three emitters were on the order of 10^6 s^{-1}, which were one or two orders of magnitude larger than those of ordinary TADF emitters (k_{RISC} ~ $10^{4–5}$ s^{-1}).[39,40] The large k_{RISC}s of **Phox-$^{MeO}\pi$** and **^{MeO3}Ph-$^{FMe}\pi$** were consistent with our design concept. In contrast, **Phox-$^{Me}\pi$** also showed an unexpectedly large k_{RISC} in spite of the fact that the ^{3}LE state of **Phox-$^{Me}\pi$** would not be involved in RISC from the calculated energy levels in Fig. 1. A possible reason is that the actual energy level of the ^{3}LE is closer to ^{1}CT and ^{3}CT than that expected from the quantum chemical calculation.

Finally, we investigated OLED performance using these three molecules as emitters. Their good solubilities encouraged us to fabricate the devices by a solution process. The device structure was as follows: ITO (50 nm)/PEDOT:PSS (45 nm)/PVK (15 nm)/5 wt% emitter: host (40 nm)/PPF (10nm)/TPBi (45 nm)/Liq (1 nm)/Al (80 nm). In these devices, indium-tin-oxide (ITO) and Al act as the anode and cathode, respectively. Poly(styrene sulfonic acid)-doped poly(3,4-ethylenedioxythiphene) (PEDOT:PSS) was employed for

Accepted Manuscript

hole injection, poly(*N*-vinylcarbazole) (PVK) for hole transport and electron blocking, PPF for hole blocking, 2,2′,2″-(1,3,5-benzinetriyl)-tris(1-phenyl-1-*H*-benzimidazole) (TPBi) for electron transport, and 8-hydroxyquinolinato lithium (Liq) for electron injection (Fig. 3a). The host materials and doping concentrations for **Phox-^{Me}π** and **Phox-^{MeO}π** were the same as used for the photophysical measurements (5 wt%), while no host material was used for **^{MeO3}Ph-^{FMe}π** (Fig. S2) because of its high Φ_{PL} (79%) in the neat film.

Figures 3(a)–3(c) illustrate the device structure, electroluminescence (EL) spectra, and EQE-luminance curves. The device performances are summarized in Table II. As shown in Fig. 3b and Table II, the devices prepared from **Phox-^{Me}π** and **Phox-^{MeO}π** exhibited EL spectra with maximum wavelengths (λ_{EL}) of 569 and 595 nm, respectively. Both EL spectra were blue-shifted compared to PL spectra due to the microcavity effect in the devices. The EQE_{max} values were 10.0% for **Phox-^{Me}π** and 6.7% for **Phox-^{MeO}π** (Fig. 3c).

The theoretical maximum EQEs ($EQE_{theo,max}$s) were calculated as follows[41]:

$$EQE_{theo,max} = \eta_p + \eta_d, \quad (2)$$

$$\eta_p = 0.25\Phi_p\gamma\Phi_{out}, \quad (3)$$

$$\eta_d = \left[0.75 + 0.25(1-\Phi_p)\right]\frac{\Phi_d}{1-\Phi_p}\gamma\Phi_{out}, \quad (4)$$

where η_p and η_d are the contributions of the prompt and delayed components to $EQE_{theo,max}$, respectively, and γ and Φ_{out} are charge recombination and light out-coupling factors, respectively. Here, $\gamma\Phi_{out}$ was assumed to be 0.2 following previous reports for solution processed OLEDs.[41] Φ_p and Φ_d represent the prompt and delayed components of Φ_{PL}, respectively. For the OLEDs based on **Phox-^{Me}π** and **Phox-^{MeO}π**, the $EQE_{theo,max}$ values are calculated to be 12.7% and 4.2%, respectively, which are in good agreement with the experimental results (Table II). From the Eqs. (2) and (3), we found that the contributions of delayed fluorescence were significant; η_p = 1.1% and η_d = 11.6% for **Phox-^{Me}π** and η_p = 1.2% and η_d = 3.0% for **Phox-^{MeO}π**, indicating that RISC plays a crucial role in achieving the high EQEs. The device performance of **^{MeO3}Ph-^{FMe}π** was poor because of the low sublimation temperature and deep HOMO level (Table SVII, Figs. S2-S4). The details are discussed in the supplementary data (page S8).

Accepted Manuscript

In summary, we have investigated photophysical and device performances of **Phox-^{Me}π**, **Phox-^{MeO}π**, and ^{MeO3}**Ph-^{FMe}π**. **Phox-^{MeO}π** and ^{MeO3}**Ph-^{FMe}π** were designed to accelerate RISC without using heavy atoms, and their k_{RISC}s were determined to be 1.6×10^6 and 2.0×10^6 s^{-1}, respectively. The efficient RISC for both emitters was due to mediation by the ^{3}LE state as designed. **Phox-^{Me}π** and **Phox-^{MeO}π**-based devices prepared by a solution process exhibited EQE_{max} values of 10.0% and 6.7%, respectively. Delayed fluorescence largely contributed to the EQEs, indicating that highly efficient RISC occurred in the devices.

Acknowledgments

This work was supported by JSPS KAKENHI grant numbers: JP20H05837 and JP20H05840 (Grant-in-Aid for Transformative Research Areas, "Dynamic Exciton"), JSPS Core-to-Core Program grant numbers: JPJSCCA20220004, and the International Collaborative Research Program of the Institute for Chemical Research, Kyoto University (grant #'s 2021-8, 2022-9, and 2023-5).

Accepted Manuscript

References

1) C. W. Tang and S. A. VanSlyke, Appl. Phys. Lett. **51**, 913 (1987).
2) R. H. Friend, R. W. Gymer, A. B. Holmes, J. H. Burroughes, R. N. Marks, C. Taliani, D. D. C. Bradley, D. A. D. Santos, J. L. Brédas, M. Lögdlund, and W. R. Salaneck, Nature **397**, 121 (1999).
3) B. Geffroy, P. le Roy, and C. Prat, Polym. Int. **55**, 572 (2006).
4) Y. Huang, E.-L. Hsiang, M.-Y. Deng, and S.-T. Wu, Light: Sci. Appl. **9**, 105 (2020).
5) M. A. Baldo, D. F. O'Brien, M. E. Thompson, and S. R. Forrest, Phys. Rev. B **60**, 14422 (1999).
6) M. Segal, M. A. Baldo, R. J. Holmes, S. R. Forrest, and Z. G. Soos, Phys. Rev. B **68**, 075211 (2003).
7) M. Pope, H. P. Kallmann, and P. Magnante, J. Chem. Phys. **38**, 2042 (1963).
8) M. Liu, X.-L. Li, D. C. Chen, Z. Xie, X. Cai, G. Xie, K. Liu, J. Tang, S.-J. Su, and Y. Cao, Adv. Funct. Mater. **25**, 5190 (2015).
9) M. A. Baldo, D. F. O'Brien, Y. You, A. Shoustikov, S. Sibley, M. E. Thompson, and S. R. Forrest, Nature **395**, 151 (1998).
10) M. A. Baldo, M. E. Thompson, and S. R. Forrest, Nature **403**, 750 (2000).
11) C. Adachi, M. A. Baldo, S. R. Forrest, and M. E. Thompson, Appl. Phys. Lett. **77**, 904 (2000).
12) X. Gong, J. C. Ostrowski, G. C. Bazan, D. Moses, and A. J. Heeger, Appl. Phys. Lett. **81**, 3711 (2002).
13) W.-Y. Wong and C.-L. Ho, J. Mater. Chem. **19**, 4457 (2009).
14) Y. Chi and P.-T. Chou, Chem. Soc. Rev. **39**, 638 (2010).
15) H. Yersin, A. F. Rausch, R. Czerwieniec, T. Hofbeck, and T. Fischer, Coord. Chem. Rev. **255**, 2622 (2011).
16) A. Endo, M. Ogasawara, A. Takahashi, D. Yokoyama, Y. Kato, and C. Adachi, Adv. Mater. **21**, 4802 (2009).
17) H. Uoyama, K. Goushi, K. Shizu, H. Nomura, and C. Adachi, Nature **492**, 234 (2012).
18) C. Adachi, Jpn. J. Appl. Phys. **53**, 060101 (2014).
19) M. A. Baldo, C. Adachi, and S. R. Forrest, Phys. Rev. B **62**, 10967 (2000).
20) K. Masui, H. Nakanotani, and C. Adachi, Org. Electron. **14**, 2721 (2013).
21) A. Niwa, S. Haseyama, T. Kobayashi, T. Nagase, K. Goushi, C. Adachi, and H. Naito, Appl. Phys. Lett. **113**, 083301 (2018).
22) J. U. Kim, I. S. Park, C.-Y. Chan, M. Tanaka, Y. Tsuchiya, H. Nakanotani, and C. Adachi, Nat. Commun. **11**, 1765 (2020).
23) M. K. Etherington, J. Gibson, H. F. Higginbotham, T. J. Penfold, and A. P. Monkman, Nat. Commun. **7**, 13680 (2016).
24) C. M. Marian, J. Phys. Chem. C **120**, 3715 (2016).
25) M. A. El-Sayed, J. Chem. Phys. **38**, 2834 (1963).
26) X.-K. Chen, D. Kim, and J.-L. Brédas, Acc. Chem. Res. **51**, 2215 (2018).
27) Y. Wada, H. Nakagawa, S. Matsumoto, Y. Wakisaka, and H. Kaji, Nat. Photonics **14**, 643 (2020).
28) C.D. Entwistle and T.B. Marder, Angew. Chem. Int. Ed. **41**, 2927 (2002).
29) C.D. Entwistle and T.B. Marder, Chem. Mater. **16**, 4574 (2004).
30) L. Ji, S. Griesbeck, and T.B. Marder, Chem. Sci. **8**, 846 (2017).
31) S.M. Berger and T.B. Marder, Mater. Horiz. **9**, 112 (2022).

Accepted Manuscript

32) S.M. Berger, M. Ferger, and T.B. Marder, Chem. Eur. J. **27**, 7043 (2021).
33) G. Zhou, C.-L. Ho, W.-Y. Wong, Q. Wang, D. Ma, L. Wang, Z. Lin, T.B. Marder, and A. Beeby, Adv. Funct. Mater. **18**, 499 (2008).
34) X. Chen, G. Meng, G. Liao, F. Rauch, J. He, A. Friedrich, T.B. Marder, N. Wang, P. Chen, S. Wang, and X. Yin, Chem. Eur. J. **27**, 6274 (2021).
35) A. K. Narsaria, F. Rauch, J. Krebs, P. Endres, A. Friedrich, I. Krummenacher, H. Braunschweig, M. Finze, J. Nitsch, F. M. Bickelhaupt, and T. B. Marder, Adv. Funct. Mater. **30**, 2002064 (2020).
36) J. Lee, N. Aizawa, and T. Yasuda, Chem. Mater. **29**, 8012 (2017).
37) Y. Wada, S. Kubo, and H. Kaji, Adv. Mater. **30**, 1705641 (2018).
38) P. A. Vecchi, A. B. Padmaperuma, H. Qiao, L. S. Sapochak, and P. E. Burrows, Org. Lett. **8**, 4211 (2006).
39) K. P. C. P, K. R. Naveen, and J. Hur, Mater. Chem. Front. **8**, 769 (2024).
40) R. Braveenth, K. Raagulan, Y.-J. Kim, and B.-M. Kim, Mater. Adv. **4**, 374 (2023).
41) J. Lee, K. Shizu, H. Tanaka, H. Nomura, T. Yasuda, and C. Adachi, J. Mater. Chem. C **1**, 4599 (2013).

Accepted Manuscript

Figure Captions

Fig. 1. Molecular structures and calculated energy diagrams of **Phox-$^{Me}\pi$**, **Phox-$^{MeO}\pi$**, and **^{MeO3}Ph-$^{FMe}\pi$**. ΔE_{ST}s and SOC matrix element values are also shown.

Fig. 2. (a) PL spectra with their photographs and (b) transient PL decay curves of 5 wt% **Phox-$^{Me}\pi$**, **Phox-$^{MeO}\pi$**, and **^{MeO3}Ph-$^{FMe}\pi$** doped films in mCBP.

Fig. 3. (a) Device structure, (b) EL spectra with photographs, and (c) EQE-luminance curves for **Phox-$^{Me}\pi$** and **Phox-$^{MeO}\pi$**-based OLEDs fabricated by a solution process.

Accepted Manuscript

Table I. Photophysical properties of 5 wt% **Phox-^{Me}π**, **Phox-^{MeO}π** and **^{MeO3}Ph-^{FMe}π** doped films in mCBP.

emitter	λ_{PL}[a] [nm]	Φ_{PL}[b] [%]	τ_{PF}[c] [ns]	τ_{DF}[c] [μs]	k_r[d] [10^6 s^{-1}]	k_{nr}[d] [10^6 s^{-1}]	k_{ISC}[d] [10^7 s^{-1}]	k_{RISC}[d] [10^6 s^{-1}]
Phox-$_{Me}$π	581	70	60.0	1.4	3.3	1.4	1.0	2.6
Phox-$_{MeO}$π	626	36	31.9	0.9	7.4	13	1.0	1.6
^{MeO3}Ph-$_{FMe}$π	484	50	82.5	3.2	0.94	0.94	0.85	2.0

[a] Photoluminescence peak wavelength (λ_{PL}). [b] Photoluminescence quantum yield (Φ_{PL}). [c] Lifetime of the prompt fluorescence (τ_{PF}) and delayed fluorescence (τ_{DF}). [d] Rate constants of radiative decay (k_r), non-radiative decay (k_{nr}), intersystem crossing (k_{ISC}), and reverse intersystem crossing (k_{RISC}).

Table II. Device performances of **Phox-^{Me}π**- and **Phox-^{MeO}π**-based OLEDs with 5 wt% concentration fabricated by solution process.

emitter	λ_{EL}[a] [nm]	CE[b] [cd A^{-1}]	PE[c] [lm W^{-1}]	EQE[d] [%]	$EQE_{theo,max}$[e] [%]
Phox-^{Me}π	569	28.3/16.4	13.5/3.6	10.0/5.8	12.7
Phox-^{MeO}π	595	12.4/4.8	3.8/0.77	6.7/2.5	4.2

[a] Electroluminescence peak wavelength (λ_{EL}) at 1 mA cm^{-2}. [b] Current efficiency (CE) at maximum/500 cd m^{-2}. [c] Power efficiency (PE) at maximum/500 cd m^{-2}. [d] External quantum efficiency (EQE) at maximum/500 cd m^{-2}. [e] Theoretical maximum EQE ($EQE_{theo,max}$).

Accepted Manuscript

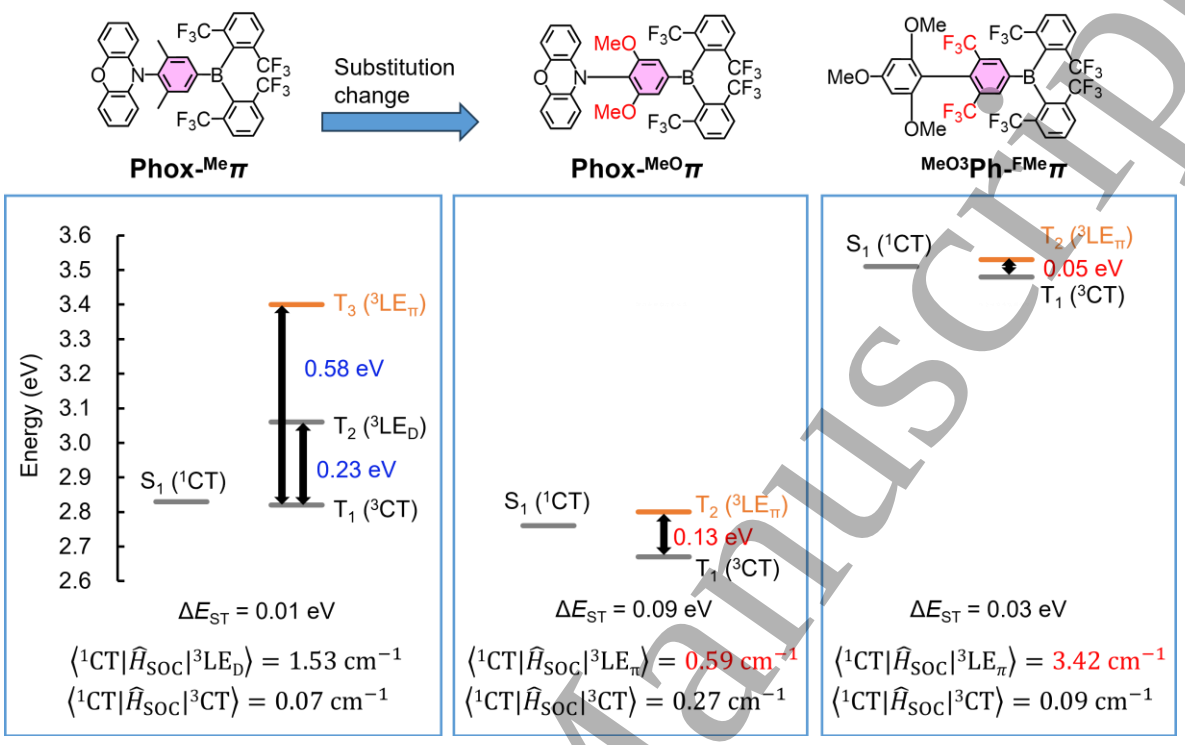

Fig. 1.

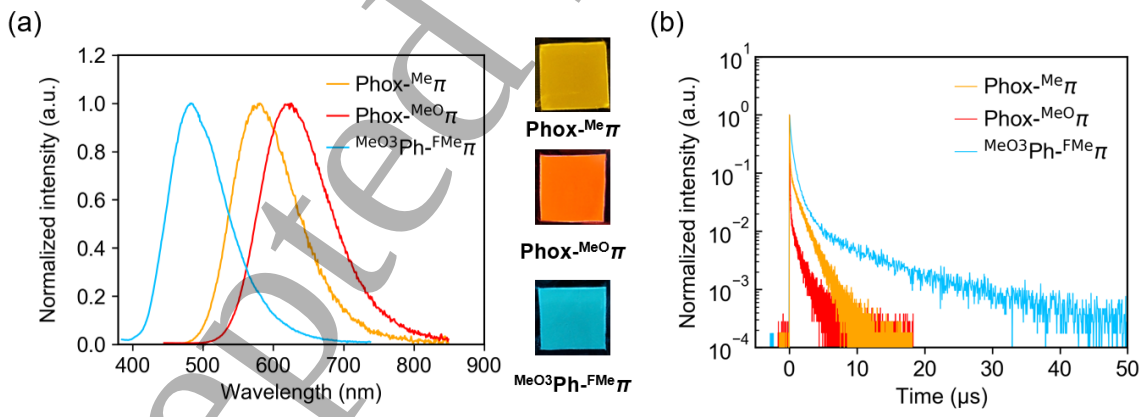

Fig. 2.

Accepted Manuscript

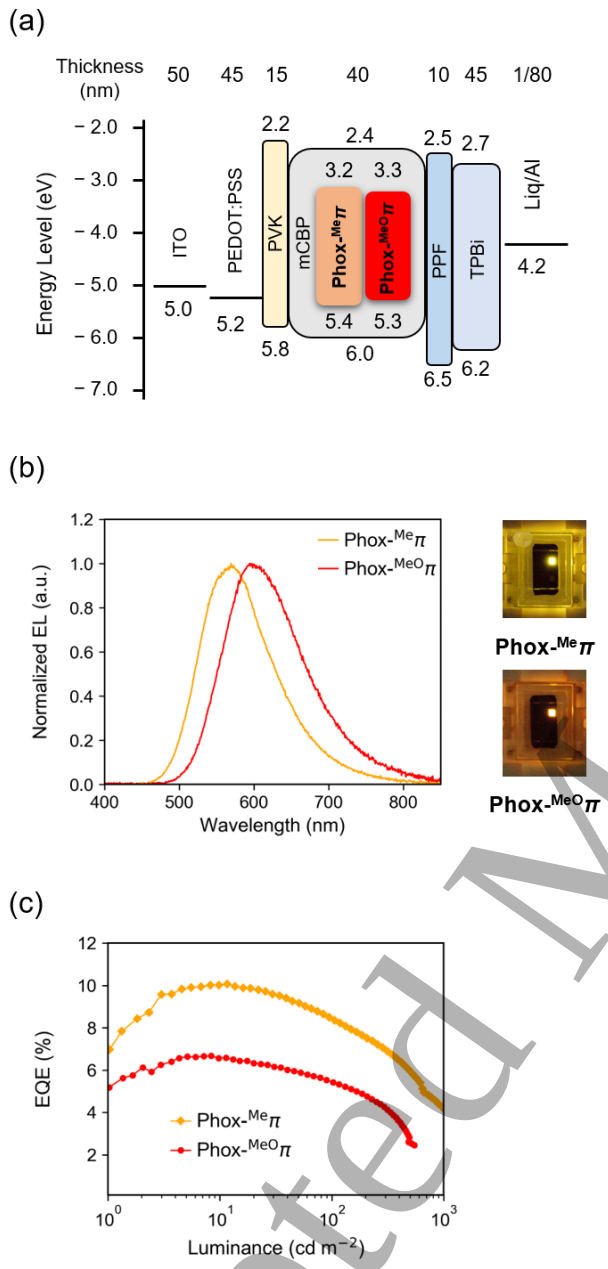

Fig. 3.

Accepted Manuscript